The Astrophysical Journal, 822:17 (7pp), 2016 May 1 doi:10.3847/0004-637X/822/1/17

GAS PHASE ABSORPTION SPECTROSCOPY OF C_{60}^+ AND C_{70}^+ IN A CRYOGENIC ION TRAP: COMPARISON WITH ASTRONOMICAL MEASUREMENTS*

E. K. Campbell[1], M. Holz[1], J. P. Maier[1], D. Gerlich[2], G. A. H. Walker[3], and D. Bohlender[4]
[1] Department of Chemistry, University of Basel, CH-4056 Basel, Switzerland; ewen.campbell@unibas.ch, mathias.holz@unibas.ch, j.p.maier@unibas.ch
[2] Department of Physics, Technische Universität, D-09107 Chemnitz, Germany; gerlich@physik.tu-chemnitz.de
[3] 1234 Hewlett Place, Victoria, BC V8S 4P7, Canada; gordonwa@uvic.ca
[4] National Research Council of Canada, Herzberg Institute of Astrophysics, 5071 West Saanich Road, Victoria, BC V9E 2E7, Canada; david.bohlender@nrc-cnrc.gc.ca
Received 2016 February 1; accepted 2016 March 17; published 2016 April 27

ABSTRACT

Recent low-temperature laboratory measurements and astronomical observations have proved that the fullerene cation C_{60}^+ is responsible for four diffuse interstellar bands (DIBs). These absorptions correspond to the strongest bands of the lowest electronic transition. The gas phase spectrum below 10 K is reported here for the full wavelength range encompassed by the electronic transition. The absorption spectrum of C_{70}^+, with its origin band at 7959.2 Å, has been obtained under similar laboratory conditions. Observations made toward the reddened star HD 183143 were used in a specific search for the absorption of these fullerene cations in diffuse clouds. In the case of C_{60}^+, one further band in the astronomical spectrum at 9348.5 Å is identified, increasing the total number of assigned DIBs to five. Numerous other C_{60}^+ absorptions in the laboratory spectrum are found to lie below the astronomical detection limit. Special emphasis is placed on the laboratory determination of absolute absorption cross-sections. For C_{60}^+ this directly yields a column density, $N(C_{60}^+)$, of 2×10^{13} cm^{-2} in diffuse clouds, without the need to rely on theoretical oscillator strengths. The intensity of the C_{70}^+ electronic transition in the range 7000–8000 Å is spread over many features of similar strength. Absorption cross-section measurements indicate that even for a similar column density, the individual absorption bands of C_{70}^+ will be too weak to be detected in the astronomical spectra, which is confirmed giving an upper limit of 2 mÅ to the equivalent width.

Key words: ISM: molecules

1. INTRODUCTION

The diffuse interstellar bands (DIBs) are seen in the spectra of stars reddened by interstellar dust. These features were first detected nearly 100 years ago (Heger 1922). Since then a number of hypotheses have been put forward as to their origin (Snow & McCall 2006). Over the last several decades, laboratory spectroscopy has been performed with the aim of identifying the molecules responsible. Progress toward this goal came with the ability to measure the gas phase electronic spectra of polyatomics, short-lived radicals, and ions at low temperatures (10–80 K). These were reported for carbon chains and ions (Rice & Maier 2013), as well as of a few polycyclic aromatic cations with absorptions in the DIB range (Snow & McCall 2006). However, none of these unambiguously matched the astronomical data.

A major breakthrough came with gas phase measurements of C_{60}^+ cooled using a cryogenic ion trap to temperatures relevant to the interstellar medium. This led to the first unequivocal identification of a molecular ion as a carrier of two DIBs (Campbell et al. 2015). The observation of two more DIBs consistent with laboratory measurements of weaker C_{60}^+ absorption bands was then reported (Walker et al. 2015). With the discovery of C_{60}^+ in the interstellar medium, long-standing interest in fullerenes (Kroto 1988) and derivatives (Kroto & Jura 1992) and their role in astrochemistry has reawakened.

Of particular importance in this context is the column density of C_{60}^+ in diffuse interstellar clouds, $N(C_{60}^+)$. This quantity has been previously estimated based on the oscillator strength, f, for the electronic transition reported by matrix isolation (Fulara et al. 1993) and theoretical (Bendale et al. 1992; Tamuliene 2014) studies. The value obtained in the neon matrix study, a factor of ten smaller than calculated, was underestimated because of ion loss during its growth. A recent experimental matrix isolation study (Strelnikov et al. 2015) reports values in accord with the theoretical predictions.

The identification of C_{60}^+ in diffuse interstellar clouds leads to the question of the role played by other fullerenes and derivatives with respect to the DIBs. The next most abundant fullerene observed in carbon soot produced in an electric arc discharge with graphite rods is C_{70} (Krätschmer et al. 1990). This molecule satisfies the isolated pentagon rule used to explain the stability of the fullerenes (Kroto 1987). Furthermore, its ionization potential is low, 8.0 ± 0.5 eV (Wörgötter et al. 1994), suggesting that in diffuse clouds, as for C_{60}, it would be in its ionized form, C_{70}^+.

In 1993 Maier and co-workers recorded the electronic spectrum of mass selected C_{70}^+ in a neon matrix (Fulara et al. 1993). The spectrum, which corresponds to the $^2E_1' \leftarrow X\ ^2E_1''$ electronic transition (in an assumed D_{5h} symmetry), shows rich vibronic structure in the range 7140–8060 Å, a region where numerous DIBs have been detected. However, aside from the origin band (at 7979 Å in solid neon) it appears complicated and congested when compared with the $A\ ^2E_g \leftarrow X\ ^2A_{1u}$ (in D_{5d} symmetry) spectrum of C_{60}^+. In the latter a significant portion of the oscillator strength for the electronic transition is localized in

* Based on observations obtained at the Canada–France–Hawaii Telescope (CFHT) which is operated by the National Research Council of Canada, the Institut National des Sciences de l'Univers of the Centre National de la Recherche Scientifique of France, and the University of Hawaii.

two strong features at 9632.7 Å and 9577.5 Å. In the matrix spectrum of C_{70}^+, however, this appears more evenly distributed among more than 20 vibronic bands.

The paper is organized as follows. In Section 2, the experimental procedure used to record the electronic spectra of C_{60}^+ and C_{70}^+ and determine the absorption cross-sections at specific wavelengths is described. The details of the astronomical observations are given in Section 3. The laboratory spectra of C_{60}^+ and C_{70}^+ are presented in Sections 4.1 and 4.2, respectively, along with a comparison with the astronomical data.

2. EXPERIMENTAL

The electronic absorption spectra of the fullerene cations were recorded by photoinduced fragmentation of C_{60}^+ – He and C_{70}^+ – He complexes. This method was used in 1990 to record the electronic spectrum of N_2^+ – He using a supersonic expansion (Bieske et al. 1990). Cryogenic radiofrequency ion traps, such as the well-characterized 22-pole (Gerlich 1993), have the advantage that they allow flexible control over the temperature and timescale for cooling. A major breakthrough in the use of these devices was achieved recently by pushing the number density of helium buffer gas to the highest and the temperature of the ions to the lowest limits. This has enabled M^+ – He complexes to be synthesized inside the trap from mass-selected, buffer-gas-cooled M^+ ions, leading to new possibilities for recording the spectra of trapped ions in the infrared (Jašík et al. 2013) and visible (Chakrabarty et al. 2013) at temperatures of just a few K.

The present results have been obtained in the cryogenic ion trap instrument described in Dzhonson et al. (2006) and Chakrabarty et al. (2013). In order to determine the absolute photoabsorption cross-sections better, the 22-pole has been replaced by a linear quadrupole trap (Figure 1). The fullerene ions C_{60}^+ and C_{70}^+ are formed by 65 eV electron impact of the neutral gas, produced by heating a solid sample to around 340°C. The internally hot ions are transmitted through a quadrupole mass filter and turned through 90° using an electrostatic quadrupole. The deflected ions are loaded into the linear quadrupole trap ($r_0 = 5$ mm, $V_0 = 150$ V, $f = 780$ kHz) which is mounted on the second stage of a closed cycle helium cryostat. The temperature of the trap walls defines the nominal temperature, $T_{\rm nom}$. The repetition rate of the trapping experiment is usually 1 Hz.

In the trap the ions undergo many inelastic collisions with helium buffer gas, introduced by resonantly exciting a piezo valve for 300 ms. Number densities of some 10^{15} cm^{-3} are sufficient for cooling all internal degrees of freedom of the fullerene ions to such a low temperature that weakly bound C_{60}^+ – He and C_{70}^+ – He species are formed. Due to the large mass of the ions in comparison with He, the rotational temperature attained is close to $T_{\rm nom}$. After a storage time of 0.5 to 1 s the trap contents are extracted, analyzed with a quadrupole mass spectrometer, and counted with a Daly detector. Typically some thousands of complexes are created per filling, with up to 30% conversion of C_{60}^+ primary ions. Complexes with several weakly bound helium atoms can also be formed.

The ions are exposed to laser radiation provided by either a titanium sapphire (Ti:Sa) or a diode laser 100 – 200 ms after closing the piezo valve. The Ti:Sa ring laser was used in the region 7300 – 9300 Å and a homebuilt diode laser for 9300 – 9650 Å. Photon absorption gives rise to electronically excited C_{60}^+ – He and C_{70}^+ – He complexes which undergo fast internal conversion. Much slower is the transfer of energy from the carbon cage into the van der Waals mode, leading finally to the loss of the helium atom. Spectra are recorded by monitoring the attenuation of the number of ions per filling, N_i, on mass 724 u (mainly $^{12}C_{60}^+$ – He) and 844 u (mainly $^{12}C_{70}^+$ – He) as a function of the laser wavelength. To account for fluctuations in the number of trapped ions the N_i are recorded alternately with and without laser radiation. The relative laser power is monitored with a photodiode located at the exit of the instrument and the resulting spectra are normalized.

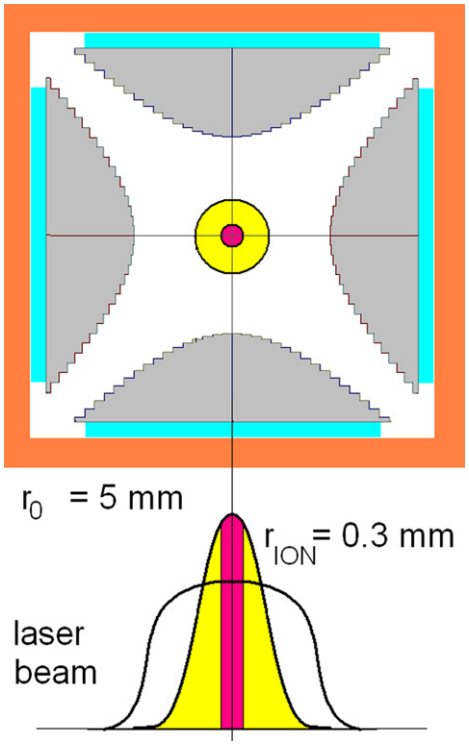

Figure 1. Geometry of the ion cloud confined in the linear quadrupole trap ($r_0 = 5$ mm) and the laser beam. The four electrodes (gray) follow the hyperbolic boundary conditions using a step function and are mounted directly on the cold copper box (orange) using thin sapphire plates (blue) for optimal cooling. The effective potential squeezes the slow ions into a cylinder with a radius of less than 0.3 mm (red area). The laser beam is transmitted through the trap either as a narrow, nearly parallel, Gaussian beam (yellow) or with a flat top profile. The power density (flux) is determined with a calibrated profile meter.

2.1. Absorption Cross-sections

The coaxial superposition of an ion cloud confined in a linear quadrupole trap and a laser beam provides a well-defined geometry for determining absolute cross-sections for photo-induced processes in ions (Jašík et al. 2015). The intensity of light, I, transmitted through a cell of length l containing molecules with a density n is described by Beer–Lambert's law,

$$I = I_0 \exp(-\sigma n l), \quad (1)$$

where I_0 is the incident intensity and σ the cross-section for absorbing a photon. Equation (1) also holds for interstellar clouds when $n\,l$ is replaced by the column density, N_C. For example, the relative intensity $I/I_0 = 0.91$ for the 9577.5 Å

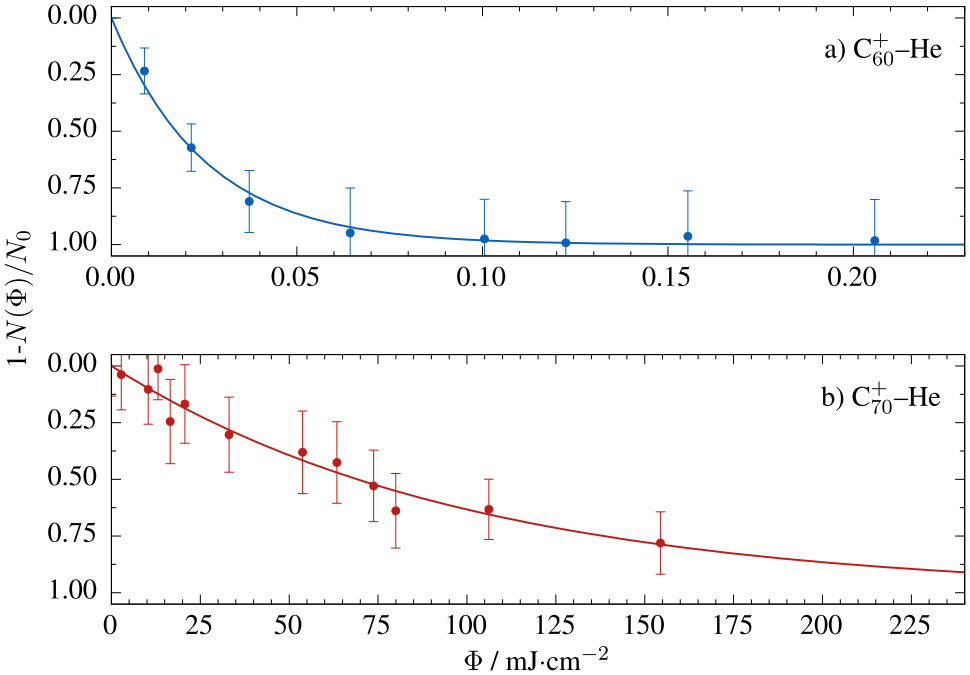

Figure 2. Fragmentation of (a) C_{60}^+ – He at 9577.5 Å and (b) C_{70}^+ – He at 7959.2 Å as a function of laser fluence. Experimental data (circles) were obtained by monitoring the number of ions as a function of laser fluence, $N(\Phi)$. The exponential fits (lines) provide information on the fragmentation cross-sections. The data have been corrected for the background ions appearing at $m/z = 724$ and 844 u/e.

interstellar absorption of C_{60}^+ was reported by Walker et al. (2015).

In the laboratory experiments the light interacts with a confined ensemble of some thousand ions leading to very small column densities and light attenuation of about 5×10^{-11} in the case of C_{60}^+ – He stored in the 22-pole. As a result direct absorption measurements, performed by monitoring the transmitted intensity of light, are difficult. Information on the absolute absorption cross-section comes instead from the fragmentation of complexes, occurring after photon absorption. A unique sensitivity is achieved by counting (almost) all of the mass-selected ions following their extraction from the trap. Under the conditions of the present experiment the quantum yield for dissociation is unity and therefore the photofragmentation and absorption cross-sections are identical.

The probability to hit an ion is proportional to the laser fluence, Φ (number of photons per cm^2), and the cross-section, σ. Integration over the ion cloud and using the mean fluence, Φ, leads to

$$N(\Phi) = N_0 \exp(-\sigma\Phi), \quad (2)$$

where N_0 is the initial number of complexes and $N(\Phi)$ those remaining after exposure to the light. The mean value of the fluence is calculated from the measured power of the laser, P, its profile at the location of the trap, and the irradiation time, Δt. In the linear quadrupole used the ion cloud is compressed and this enables good superposition with the laser beam, as illustrated in Figure 1.

The number of complexes is measured at several fluencies by varying the laser power or the irradiation time with all other experimental parameters (e.g., geometry, rf amplitude, He density) unchanged. Typical results for the origin bands of the C_{60}^+ and C_{70}^+ electronic transitions are shown in Figure 2. The obtained data are fitted to the exponential function

$$N(\Phi) = N_0 \exp(-\Phi/\Phi_0) + N_1. \quad (3)$$

At high laser fluence, the curves decrease to a common asymptotic value, N_1, which is due to the number of $^{13}C_4^{12}C_{56}$ ($^{13}C_4^{12}C_{66}$) background ions appearing at $m/z = 724$ (844) u/e. Comparison of Equations (2) and (3) reveals that the derived characteristic fluence, Φ_0, can be directly converted into the cross-section, σ,

$$\sigma = 1/\Phi_0. \quad (4)$$

The most reliable cross-sections were obtained using a laser profile with a flat top of diameter 3.2 mm, an irradiation time of 12 ms, and powers of a few mW or even lower for C_{60}^+. The characteristic fluence for the C_{60}^+ – He origin band at 9577.5 Å is determined to be $\Phi_0 = 45\ \mu$J cm^{-2} which corresponds to an absorption cross-section of $(4.6 \pm 0.2) \times 10^{-15}$ cm^2, where the indicated error is the statistical uncertainty. After taking into account the larger systematic uncertainties of the experiment (laser power 5%, mean area 30%, irradiation time 20%, reproducibility of the laser-ion cloud overlap 30%, background N_1 10%) the cross-sections are determined to be

$$\sigma(C_{60}^+, 9577.5\ \text{Å}) = (5 \pm 2) \times 10^{-15}\ \text{cm}^2$$
$$\sigma(C_{70}^+, 7959.2\ \text{Å}) = (7 \pm 3) \times 10^{-18}\ \text{cm}^2.$$

3. ASTRONOMICAL OBSERVATIONS

Comparison with astronomical observations is based on high-quality spectra of the reddened B star HD 183143 taken with the ESPaDOnS spectrograph (Donati 2003) fiber fed from the CFH 3.6 m telescope. Spectral resolution is approximately 65,000, or 0.05 Å per pixel. There are two gaps in the ESPaDOnS spectral coverage in the region of the C_{60}^+

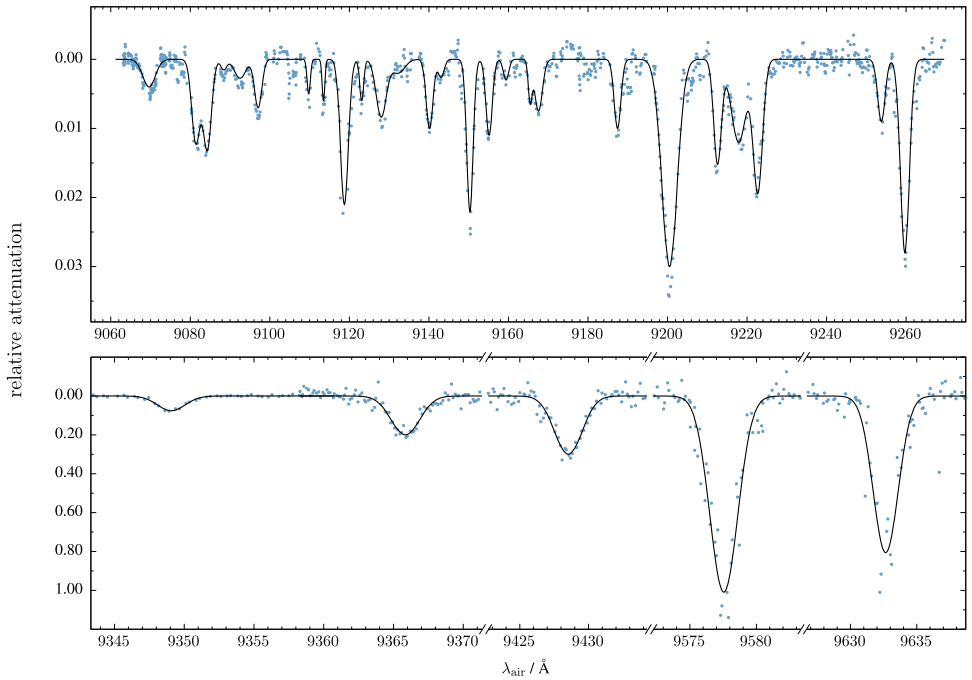

Figure 3. Absorptions of C_{60}^+ in the gas phase recorded by monitoring the depletion on the $m/z = 724$ mass channel. Gaussian fits to the experimental data (circles) are the solid lines. The intensities of the bands have been scaled by the relative absorption cross-sections which are normalized to the strongest band at 9577.5 Å. The five strongest bands shown in the lower panel have now been detected as diffuse interstellar bands.

laboratory bands between 9224 – 9234 Å and 9608 – 9636 Å where the échelle orders lie beyond the edge of the detector. The latter gap prevents detection of the 9632.7 Å band.

Telluric water lines (WV) seriously contaminate the spectral regions covered by the laboratory bands for C_{60}^+ (see Figure 1 in Walker et al. 2015). To first order, these can be eliminated by normalization using spectra of an unreddened, rapidly rotating star taken at the same air mass. Rapid rotation results in broad, shallow stellar lines which, in the normalization, appear as weak, broad "emission" features thereby minimizing any impact when fitting continua. An unreddened standard matching as closely as possible the spectral type and luminosity of the reddened target star was also observed to correct for weak stellar features. Details of HD 183143 and the standard stars are given in Table 1 of Walker et al. (2015).

The observations of HD 183143 and standards were made on the night of 2015 July 28 UT. Full details of the reductions are given in Walker et al. (2015). Attempts to correct for WV by chopping between the target and the WV standard were not entirely successful as significant residuals for the stronger WV lines remain. In addition, the spectral standard used was not a close match resulting in residual absorption and emission features in the final ratios (see, for example, the 9428.5 Å panel in Figure 2 of Walker et al. 2015).

For the region covered by the laboratory C_{70}^+ bands, the telluric A band of O_2 blanks out the range 7600 – 7660 Å preventing scrutiny for bands of <1% depth, in particular the strongest laboratory band at 7632.6 Å.

4. RESULTS AND DISCUSSION

4.1. Laboratory and Astronomical Spectra: C_{60}^+

The C_{60}^+ absorption spectrum, measured via the fragmentation of C_{60}^+ – He in the region 9000 – 9700 Å, is presented in Figure 3. Measurements of the origin band for C_{60}^+ – He_2 indicate that the perturbation on the electronic transition due to the presence of the weakly bound helium atom is very small, <0.2 Å, such that the spectrum may be considered as that of C_{60}^+ for comparison with astronomical data (Campbell et al. 2015). The individual bands have been fitted with Gaussian functions, following the typical evaluation of astronomical data, giving the parameters listed in Tables 1 and 2.

Inspection of the relative attenuation scale of Figure 3 reveals that the electronic transition of C_{60}^+ is dominated by the two strong bands at 9632.7 Å and 9577.5 Å which were first identified in diffuse interstellar clouds by Foing & Ehrenfreund (1994). The next two bands to shorter wavelength, at 9428.5 Å and 9365.9 Å, are more than a factor of 3 weaker than the 9577.5 Å band but have still been detected as DIBs in the interstellar spectrum of HD 183143 and HD 169454, as reported by Walker et al. (2015).

The next laboratory absorption to shorter wavelength is at 9349.1 Å with an intensity of only around 7% of the strong band at 9577.5 Å. A DIB matching the characteristics of this weak laboratory feature is reported here in observations toward HD 183143. The astronomical and laboratory spectra are compared in Figure 4. For the purpose of Table 1, the interstellar spectrum in the region covering the laboratory absorption at 9349.1 Å has been fit with two Gaussians due to the overlap of the C_{60}^+ band with a nearby interstellar feature of similar magnitude (Figure 4). As a result, in addition to having a depth of less than 1%, the presence of the companion DIB contributes to uncertainty in the listed position and width. It should be noted that the errors for the astronomical data are from the Gaussian fit but the actual uncertainty is certainly larger.

The laboratory C_{60}^+ spectrum shown in the upper panel of Figure 3 has a complicated pattern of weaker transitions toward shorter wavelengths, reflecting the vibronic and Jahn–Teller

Table 1
Laboratory and Interstellar C_{60}^+ Bands[a]

Laboratory			Interstellar			
λ_c/Å	FWHM/Å	σ_{rel}[b]	λ_c[c]/Å	FWHM/Å	Depth/%	Source
9632.7 ± 0.1	2.2 ± 0.2	0.8	9632.6 ± 0.2	3.0 ± 0.2	…[d]	Jenniskens et al. (1997)
9577.5 ± 0.1	2.5 ± 0.2	1	9577.4 ± 0.02	3.3 ± 0.04	9.1 ± 0.05	Walker et al. (2015)
9428.5 ± 0.1	2.4 ± 0.1	0.3	9428.4 ± 0.1	3.2 ± 0.1	…[e]	Walker et al. (2015)
9365.9 ± 0.1	2.4 ± 0.1	0.2	9365.7 ± 0.02	2.5 ± 0.04	2.4 ± 0.03	Walker et al. (2015)
9349.1 ± 0.1	2.3 ± 0.2	0.07	9348.5 ± 0.13	1.4 ± 0.2	0.5 ± 0.08	This work

Notes.
[a] Central (air) wavelengths (λ_c), depths and FWHM from Gaussian fits to the lab and astronomical bands. The quoted errors for the astronomical data from Walker et al. (2015) and this work are merely from the Gaussian fits but the systematic uncertainties are certainly larger.
[b] Relative cross section.
[c] Corrected by -12 km s^{-1} for the interstellar K line off-set for HD 183143.
[d] A gap in the spectral coverage containing the laboratory absorption at 9632.7 Å prevented detection of the interstellar band in observations toward HD 183143 (Walker et al. 2015). This DIB has been reported several times previously (see, for example, Foing & Ehrenfreund 1994, 1997).
[e] A stellar emission feature at 9429 Å prevented detection of the laboratory absorption at 9428.5 Å in observations toward HD 183143. The band has been detected in the spectrum of HD 169454 (Walker et al. 2015).

Table 2
Laboratory C_{60}^+ Bands[a]

λ_c[b]/Å	FWHM[c]/Å	σ_{rel}[d]	λ_c[b]/Å	FWHM[c]/Å	σ_{rel}[d]
9259.6	2.7	0.03	9140.2	2.0	0.01
9253.8	2.3	0.01	9128.0	3.0	0.01
9222.7	2.7	0.02	9118.7	2.3	0.02
9212.6	2.1	0.02	9097.1	2.2	0.01
9200.5	3.7	0.03	9084.3	2.5	0.01
9155.1	1.9	0.01	9081.4	2.5	0.01
9150.3	2.6	0.02	…	…	…

Notes.
[a] Wavelengths in air, λ_c, and FWHM determined by Gaussian fits to the laboratory spectrum of C_{60}^+ shown in the upper panel of Figure 2. σ_{rel} are relative to 9577.5 Å (see Table 1), weak absorptions with $\sigma_{rel} \leqslant 0.01$ are not included.
[b] Band positions are given with an uncertainty of ±0.2 Å.
[c] σ_{rel} are listed with an estimated uncertainty of around 20%.
[d] FWHM should be considered as an upper limit (see text).

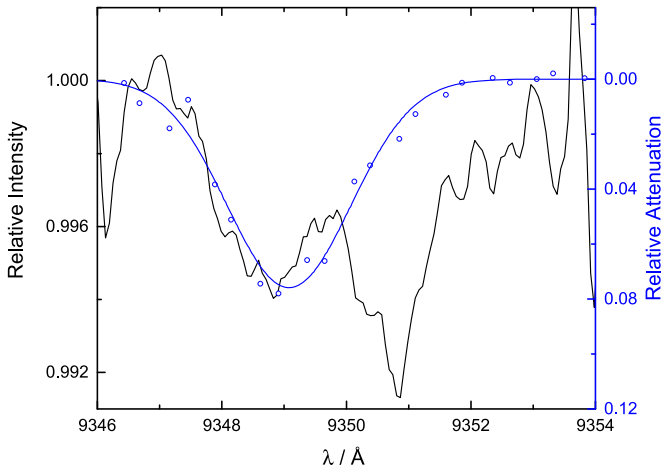

Figure 4. Comparison of laboratory (blue) and astronomical (black) data in the region of the C_{60}^+ absorption at 9349.1 Å. The solid blue curve is a Gaussian fit to the laboratory band. The astronomical data is from observations toward HD 183143. A similar weak interstellar band is also observed near 9351 Å. Details of the telluric water line removal are given in the text.

couplings present. In order to determine the wavelengths of the weak bands in this region, the spectrum was recorded in the nonlinear regime using higher laser fluence. This leads to an experimentally observed broadening of the bands (Campbell et al. 2015). Thus the values listed in Table 2 should be considered as upper limits to the natural width.

The equivalent width (EW) of the 9577.5 Å C_{60}^+ DIB is around 300 mÅ (Walker et al. 2015). The relative intensities of these weak C_{60}^+ laboratory bands (Figure 3, upper panel) indicates that the corresponding DIBs would have EWs in the range of just a few mÅ and therefore be difficult to detect. After correction for telluric lines, the signal-to-noise ratio (S/N) for the HD 183143 spectra in the region of 9577 Å is 300 per pixel or 1500 per Å. For a band with a 2.5 Å FWHM this gives a 3σ EW detection limit of 3 mÅ.

The gas phase absorption cross-section and astronomical observations can be used to determine the column density of C_{60}^+ in diffuse clouds directly. The column density is given by $\ln(I_0/I)/\sigma$, where I represents the intensity of the light transmitted by the interstellar cloud. Walker et al. (2015) reported $I/I_0 = 0.91$ for the 9577.5 Å band of C_{60}^+ following observations toward the reddened star HD 183143. Together with the measured cross-section of $(5 \pm 2) \times 10^{-15}$ cm^2 this leads to a column density of $(2 \pm 0.8) \times 10^{13}$ cm^{-2}.

4.2. Laboratory and Astronomical Spectra: C_{70}^+

The C_{70}^+ absorption spectrum, measured via the fragmentation of C_{70}^+ – He in the region 7000–8000 Å, is shown in Figure 5. The individual bands have been fitted with Gaussian functions giving the wavelengths and FWHMs listed in Table 3. The weaker bands have been evaluated in the linear regime (attenuation <20%). The stronger absorption bands of C_{70}^+ may be partly saturation broadened in addition to their natural width. The electronic transition has been previously assigned as $^2E_1' \leftarrow X\ ^2E_1''$ in D_{5h} symmetry (Fulara et al. 1993).

The origin band of C_{70}^+ – He_2 was also recorded to provide information on the perturbation of the electronic transition of C_{70}^+ due to the presence of the weakly bound helium atom. This yields band maxima ($\sim \pm$ 0.4 Å) at 7959.2 Å and 7958.8 Å for C_{70}^+ – He and C_{70}^+ – He_2, respectively. Thus, as in the case of

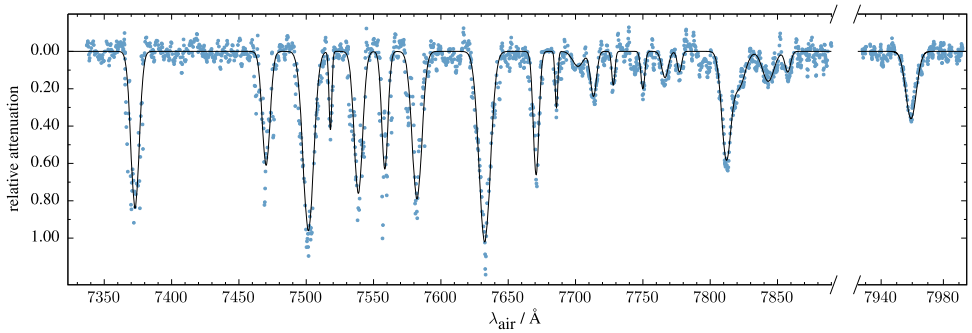

Figure 5. Absorptions of C_{70}^+ in the gas phase recorded by monitoring the depletion on the $m/z = 844$ mass channel. Gaussian fits to the experimental data (circles) are the solid lines. The intensities of the bands have been scaled by the relative absorption cross-sections which are normalized to the strongest band at 7632.6 Å

Table 3
Laboratory C_{70}^+ Bands[a]

λ_c [b]/Å	FWHM[d]/Å	σ_{rel} [c]	λ_c [b]/Å	FWHM[d]/Å	σ_{rel} [c]
7959.2	8.0	0.4	7685.8	2.3	0.3
7857.6	4.9	0.1	7670.7	5.0	0.7
7843.1	10.0	0.2	7632.6	10.0	1.0
7821.3	10.6	0.2	7582.3	8.6	0.8
7811.9	8.0	0.6	7558.4	5.4	0.6
7777.2	3.8	0.1	7538.7	7.4	0.8
7766.4	5.7	0.1	7518.0	2.4	0.4
7750.0	3.5	0.2	7501.6	9.3	1.0
7728.1	2.9	0.2	7470.2	6.9	0.6
7713.3	5.2	0.2	7372.8	7.3	0.9
7701.9	9.3	0.1	…	…	…

Notes.
[a] Wavelengths in air, λ_c, and FWHM determined by Gaussian fits to the laboratory spectrum of C_{70}^+ shown in Figure 5.
[b] Band positions are given with an uncertainty of ±1 Å.
[c] σ_{rel} are quoted with an estimated uncertainty of around 20%.
[d] FWHM should be considered as an upper limit (see text).

C_{60}^+, the C_{70}^+ – He photofragmentation spectrum is, for astrophysical purposes, the laboratory absorption of C_{70}^+.

The production of ions in the source leads to a huge C_{60}^+ or C_{70}^+ rotational angular momentum. However, under the conditions of the experiment, with helium number densities of some 10^{15} cm^{-3}, there are millions of collisions prior to the spectroscopic measurement. The mean values of the FWHM given in Tables 2 and 3, are 2.5 Å and 6.5 Å for C_{60}^+ and C_{70}^+, respectively, indicating a significant difference between them. The narrowest width measured is 1.9 Å while the broadest reaches 10.6 Å. In comparison the rotational envelope is estimated to be 1 Å at the temperature of the trapped ions, indicating that all lines are lifetime broadened due to internal conversion. According to simulations (Edwards & Leach 1993) the rotational profile would exceed 2.5 Å only at temperatures above 30 K. The implication is that for C_{60}^+ the excited electronic state lifetimes are between 1.2 and 2.3 ps while for C_{70}^+ these range from 0.3 to 1.4 ps.

Unlike the absorption spectrum of C_{60}^+ (Figure 3), in which the two strong origin bands at 9632.7 Å and 9577.5 Å provide a major contribution to the oscillator strength, the system of C_{70}^+ consists of many overlapping transitions of roughly equal intensity. The origin band at 7959.2 Å is a factor of 2–3 weaker than the strongest absorption at 7632.6 Å (Figure 5). The absorption cross-section at 7959.2 Å is determined to be $(7 \pm 3) \times 10^{-18}$ cm^2. Even under the assumption that the column density of C_{70}^+ is the same as for C_{60}^+, the expected depth in the astromomical spectrum due to absorption at 7632.6 Å is only 0.04%. For comparison, the strong C_{60}^+ absorption at 9577.5 Å has a depth of 9.1% in observations toward HD 183143 (Walker et al. 2015).

None of the the laboratory bands of C_{70}^+ could be detected in the spectra of HD 183143. The S/N per pixel in the region of 7700 Å was 1100 or 5000 per Å. For a typical band of 8 Å FWHM this sets a 3σ EW detection limit of 2 mÅ.

5. CONCLUSIONS

The measurement of the C_{70}^+ spectrum in the laboratory provides insight into the role played by other fullerene cations, in addition to C_{60}^+, with respect to the DIBs. Both C_{60} and C_{70} have been detected via infrared emission in a young planetary nebula (Cami et al. 2010), and since then in a variety of other environments (see, for example, Roberts et al. 2012 and references therein). Thus the presence of C_{70}^+ is also expected in the diffuse medium. However, because the intensity of the C_{70}^+ electronic transition is more evenly divided among the individual bands than for C_{60}^+, only weak DIBs are expected. A similar situation may prevail for other fullerene cations with lower symmetry than C_{60}^+, implying that they will not be the carriers of the strongest DIBs. Therefore, chemically bound derivatives of C_{60}^+ with hydrogen $C_{60}^+H_m$ and abundant interstellar metals C_{60}^+M (Kroto & Jura 1992) may prove to be the more relevant species to characterize in future laboratory studies.

REFERENCES

Bendale, R. D., Stanton, J. F., & Zerner, M. C. 1992, CPL, 194, 467
Bieske, E. J., Soliva, A., Welker, M. A., & Maier, J. P. 1990, JChPh, 93, 4477
Cami, J., Bernard-Salas, J., Peeters, E., & Malek, S. E. 2010, Sci, 329, 1180
Campbell, E. K., Holz, M., Gerlich, D., & Maier, J. P. 2015, Natur, 523, 322
Chakrabarty, S., Holz, M., Campbell, E. K., et al. 2013, JPhCh Lett., 4, 4051
Donati, J.-F. 2003, in ASP Conf. Ser. 307, Solar Polarization, ed. J. Trujillo-Bueno, & J. Sanchez Almeida (San Francisco, CA: ASP), 41
Dzhonson, A., Gerlich, D., Bieske, E. J., & Maier, J. P. 2006, JMoSt, 795, 93
Edwards, S. A., & Leach, S. 1993, A&A, 272, 533
Foing, B. H., & Ehrenfreund, P. 1994, Natur, 369, 296
Foing, B. H., & Ehrenfreund, P. 1997, A&A, 317, L59
Fulara, J., Jakobi, M., & Maier, J. P. 1993, CPL, 211, 227
Fulara, J., Jakobi, M., & Maier, J. P. 1993, CPL, 206, 203
Gerlich, D. 1993, J. Chem. Soc. Faraday Trans., 89, 2199
Heger, M. L. 1922, LicOB, 10, 146
Jašík, J., Gerlich, D., & Roithová, J. 2015, JPCA, 119, 2532
Jašík, J., Žabka, J., Roithová, J., & Gerlich, D. 2013, IJMSp, 354–355, 204
Jenniskens, P., Mulas, G., Porceddu, I., & Benvenuti, P. 1997, A&A, 327, 337

Krätschmer, W., Lamb, L. D., Fostiropoulos, K., & Huffman, D. R. 1990, Natur, 347, 354
Kroto, H. W. 1987, Natur, 329, 529
Kroto, H. W. 1988, Sci, 242, 1139
Kroto, H. W., & Jura, M. 1992, ARA&A, 263, 275
Rice, C., & Maier, J. P. 2013, JPCA, 117, 5559
Roberts, K. R. G., Smith, K. T., & Sarre, P. J. 2012, MNRAS, 421, 3277
Snow, T. P., & McCall, B. J. 2006, ARA&A, 44, 367
Strelnikov, D., Kern, B., & Kappes, M. M. 2015, A&A, 584, A55
Tamuliene, J. 2015, FNCN, 23, 187
Walker, G. A. H., Bohlender, D. A., Maier, J. P., & Campbell, E. K. 2015, ApJL, 812, L8
Wörgötter, R., Dünser, B., Scheier, P., & Märk, T. D. 1994, JChPh, 101, 8674